ContactLess Integrated Photonic Probe for light monitoring in indium phosphide-based devices

Daniele Melati ✉, *Marco Carminati, Stefano Grillanda, Giorgio Ferrari, Francesco Morichetti, Marco Sampietro, Andrea Melloni*

Dipartimento di Elettronica, Informazione e Bioingegneria, Politecnico di Milano, via Ponzio 34/5, Milano, Italy
✉ *E-mail: daniele.melati@polimi.it*

Received on 10th November 2014
Revised on 7th April 2015
Accepted on 30th April 2015

1 Introduction

Since the early beginning of photonics there has been a continuous and constant development towards larger scale of integration [1, 2]. This pressing request has brought unavoidably to a rapid shrink of the physical dimensions of each integrated device. In particular, the investigation of high index contrast technologies allowed to accommodate a larger number of components on small areas and consequently gave rise to complex and innovative circuits [3, 4].

On the other hand, the realisation and use of advanced circuits poses immediately the problem of control and stabilisation, since fabrication tolerances, fluctuations and crosstalk (thermal, electrical or optical) can continuously change the optimal working point of the circuit [5, 6]. Real-time local monitoring is hence needed to counteract these spurious effects and lock the circuit at the desired state [7]. Moreover, the techniques to actively control and change the circuit responses [8] would largely benefit from the possibility to easily and dynamically probe the working point of the circuits.

For indium phosphide (InP)-based technological platforms, the possibility to monolithically integrate complex circuits comprising sources, amplifiers and detectors together with passive circuitry as power splitters, waveguides or filters makes the problem of control a particularly critical aspect. This issue is classically solved by tapping part of the power from waveguides in few selected points and exploiting photodiodes, easily integrated in InP technologies [1]. Although powerful and applicable to many situations, this approach has an intrinsic limitation in the number of tapping points that can be placed in a single circuit without severely affecting its functionality. In a perspective of a constant increase of the circuit complexity, involving hundreds or thousands of single building blocks, light tapping would imply unsustainable waste of optical power and non-invasive light monitoring is hence a precious feature. Further, transparent monitoring of light in optical waveguides would enable the realisation of complex functionalities not achievable with conventional detectors [9].

In previous works [10, 11], we recently proposed a contactless integrated photonic probe (CLIPP) as an innovative and viable solution to overcome the problem of transparent light monitoring on silicon on insulator platforms. The CLIPP monitors the light-dependent variations of the electric conductivity of the semiconductor waveguide core that are induced by a surface-states carrier generation effects [10]. A capacitive access to the waveguide is exploited avoiding a direct contact between the CLIPP and the waveguide core, ensuring transparent operation.

In this work, we demonstrate that the CLIPP can be implemented also in InP-based technologies. We also introduce an innovative geometry for the CLIPP that uses a vertical rather than co-planar approach. The very small (although finite) conductivity of the passive semi-insulating InP substrate allows to contact directly the back side of the chip, used as a common electrode. Since a single metal strip on the waveguide is required instead of an electrode pair [10, 11], this geometry would enable a reduction of the overall CLIPP size. Finally, the CLIPP is realised without any modification to the existing technological platform offered by the foundry, thus making it suitable for the introduction in a generic foundry scheme.

The paper is organised as follows. Section 2 describes the realisation of the CLIPP device on InP-based waveguides. The vertical sensing approach is presented along with its equivalent electrical model. The characterisation of the sensor response and its application as in-line power monitor are presented in Section 3. Lastly, Section 4 reports on the results obtained in the extraction and analysis of the transfer function of a ring resonator coupled to an external Fabry–Pérot cavity using a CLIPP directly placed within the ring cavity.

2 CLIPP device on InP technology: vertical sensing approach

The InP-based optical waveguide exploited for the fabrication of the device is a 2 μm-wide rib-shaped waveguide, whose scheme is shown in Fig. 1*a*. The InGaAsP core is 1 μm high with an etch depth of 600 nm. The InP substrate has a thickness of more than 250 μm. The entire layer stack is highly Fe-doped, guaranteeing a semi-insulating behaviour with a carrier concentration comprised

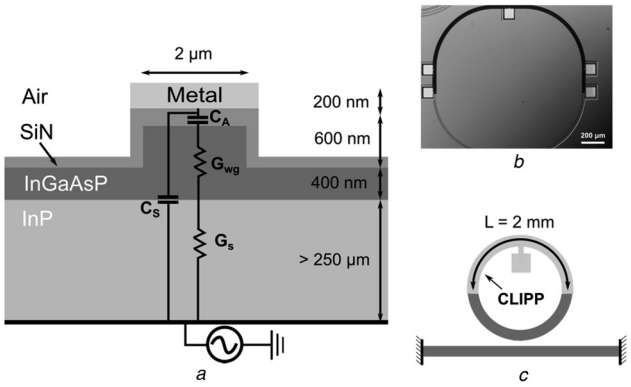

Fig. 1 *Vertical approach for the CLIPP on InP-based waveguide*

a Rib waveguide cross-section with SiN isolation layer and CLIPP metal electrode. Second electrode is realised contacting the bottom of the chip
b Photograph of the realised ring resonator with integrated vertical CLIPP
c Schematic of the device

between 10^7 and 10^8 cm^{-3}. The small residual conductivity of the stack allows to realise the CLIPP exploiting a vertical rather than coplanar approach. The bottom of the chip, which is used as a large common electrode, is directly contacted through a metallic holder and does not require a dedicated metallisation of the back side of the sample. The second metal electrode of the CLIPP seats on the top of the waveguide. A SiN isolation layer is placed between the waveguide core and the metal strip, but any other electrically insulating layer (e.g. BCB polymer) would provide the required capacitive access to the waveguide.

The realised device (Figs. 1*b* and *c*) is an all-pass ring resonator with physical length of 3.763 mm. A two-mode interference coupler [12] is used to couple the ring to the bus waveguide with a coupling factor comprised between 20 and 25%, as measured in dedicated test structures. The top electrode of the CLIPP is placed inside the ring resonator and has a length L of about 2 mm. Although several pads are present along the metal strip, only the top one was used to contact the electrode by means of a micro probe. With this scheme the CLIPP can directly monitor the optical power circulating in the cavity. As demonstrated in the next sections, this allows to monitor variations of the amount of power coupled in the bus waveguide through the input fibre and also to characterise the optical transfer function of the ring.

From the electrical point of view, the small-signal lumped equivalent circuit which models the device is illustrated in Fig. 1*a*. The SiN layer represents an insulating barrier between the top metal and the waveguide core, thus being modelled as a capacitance C_A, whose value can be estimated as a vertical parallel plate capacitor $C_A = \varepsilon_0 \varepsilon_r wL/t$, where ε_r and t are the dielectric constant and the thickness of the dielectric layer, respectively, w is the waveguide and L is the length of the top electrode. For this device C_A results to be about 2 pF. The conductance G_{wg} of the waveguide core and G_s of the substrate are in series to C_A. The total conductance G is determined by the pyramidal volume of the semiconductor in which the current flows, from the large bottom electrode to the micrometric top contact. G is largely dominated by the conductance of the core and can be approximated as $G \simeq G_{wg} = \sigma Lw/d$, where σ is the InP conductivity and d is the core thickness. Finally, an additional capacitor C_S must be added to the equivalent model in order to take into account the direct parasitic capacitive coupling between the two electrodes. In the actual setup, efforts have been devoted to the minimisation of the stray C_S (determined by the setup and in particular by the connections between the microprobes and detection instrumentation) by using distant and short shielded cables, thus obtaining $C_S \sim 0.5$ pF. This value represents, however, the dominating term in the global admittance at electrical frequencies higher than 10 kHz. Being independent of the light intensity, the effect of C_S can be removed by differential measurements.

The operation of the CLIPP is based on a variation of the waveguide conductivity induced by a change of the light intensity guided by the waveguide. Even if a variety of physical mechanisms could be responsible for this variation, some can be excluded based on the reported experimental evidences. Since the observed relation between input power and variations of G_{wg} is sub-linear (see next Fig. 2*c*), an increased carrier density because of two-photon absorption can be excluded; temperature-related mechanisms cannot explain the observed conductivity change. For a 1°C variation of the temperature, a value of $\Delta G = 0.18$ nS was measured (in absence of light by controlling the chip temperature through a thermo-optic cooler). This would imply a temperature variation because of guided light of about 5°C to change the conductivity of the waveguide of 1 nS. This temperature variation is not compatible with a guided optical power of −10 dBm as reported in Fig. 2*c*. As already demonstrated for the silicon-based monitor [10], also for InP-based CLIPP, the presence of additional photo-generated carries because of surface-state absorption along the interfaces of the waveguide is the best candidate to explain the increase of G_{wg} related to an increase of the optical power in the waveguide.

The described equivalent impedance model is conceptually identical to that adopted for silicon waveguides [10] and the reader

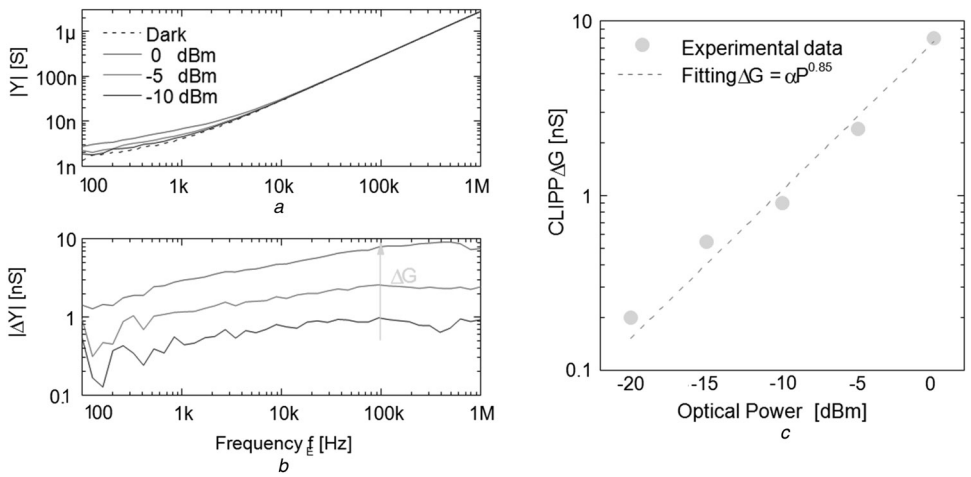

Fig. 2 *CLIPP electrical characterisation*

a Magnitude of admittance power spectra $Y(f_E)$ for different power levels in the ring cavity
b Extraction of the light-dependent increase of the conductance ΔG as difference with the dark spectrum allows to build the sensor response curve
c Sensor response curve

is addressed to this paper for more details. However, a significant difference exists between the two CLIPP structures that is noteworthy to be highlighted here. While in [10], the conductivity probe structure is horizontal along the waveguide segment, here a vertical configuration is used, that is, transversal to the waveguide direction, that implies a different dependence of G_{wg} on the device layout. In the vertical structure, once the waveguide width has been fixed ($w = 2$ μm in the realised device), only the top electrode length L is available as design parameter, determining at the same time the values of C_A and G_{wg}. As stated before, both C_A and G_{wg} linearly increase with L, so that the operational frequency of the excitation signal used to perform the measurement $f_E = 1/(2\pi C_A/G_{wg})$ is independent of the CLIPP size. This significantly simplifies the design of the CLIPP layout. In contrast, in the horizontal structure, while C_A increases with L, G_{wg} has an inverse dependence on L [10], thus resulting in an intrinsic trade-off between compactness and operating frequency [11].

Other InP-based technologies different from that considered in this work exploit a waveguide cross-section with a few-micron-thick top cladding and a sub-micron-thick core [1]. For these structures, the equivalent impedance model would be slightly different and two other series contribution to the total conductance of the stack should be considered (because of the cladding and to the etched InP section below the core), roughly with value comparable to G_{wg}. The value of the total conductance G of the stack would hence be proportionally smaller and the minimum operative frequency f_E to shunt the access capacitance would decrease accordingly (see Section 3). In any case, assuming that the largest variation to the conductivity because of the light occurs in the waveguide core, we expect no major change to CLIPP implementation and functionality with respect to the technology exploited in this work.

3 Waveguide light monitoring

To probe the conductivity G_{wg} of the InP waveguide, a sinusoidal excitation signal $V_E = 1$ V was applied to the large bottom electrode. The measurement requires the access capacitance C_A to be negligible with respect to the waveguide impedance, that is the operational frequency f_E has to be sufficiently high to shunt C_A, that is, above the pole $f_E > 1/(2\pi C_A/G_{wg}) \simeq 1$ kHz. The top electrode, acting as sensing point, was connected to a transimpedance amplifier (TIA) with gain 10^4 V/A and bandwidth 8 MHz. The TIA converts the current I_E collected at the sensing electrode into a voltage which is fed to a lock-in demodulator for in-phase and in-quadrature measurement of the overall complex impedance Z of the structure. The measured signal is proportional, through the gain of the acquisition chain, to the admittance $Y = 1/Z$ and thus to the conductivity $G = \mathrm{Re}\{Y\}$.

The first characterisation of the CLIPP has been performed by means of admittance spectroscopy, that is, by measuring the total admittance Y in the range between 100 and 1 MHz (Fig. 2*a*). Admittance spectra were measured for a set of different power levels (from −20 to 0 dBm estimated in the ring cavity) and in the case of light absence (dark spectrum in Fig. 2*a*, black dashed line). The dark spectrum was used as reference to obtain differential spectra $\Delta Y(f_E)$ (Fig. 2*b*) that allow to highlight the effect of the guided light on the waveguide admittance and to measure the variation of the conductivity $\Delta G_{wg} \simeq \Delta G = \mathrm{Re}\{\Delta Y\}$ with light intensity (assuming a constant G_s). A resistive region (flat admittance magnitude, minimum phase), which can be used to reliably measure ΔG, can be identified in a defined frequency range: for lower frequencies the impedance of C_A cannot be neglected; at higher frequencies C_S dominates and amplifies any drifting difference with respect to the dark reference spectrum, thus reducing the sensitivity of the measurement. In this case, this range is comprised between $f_E = 100$ kHz and $f_E = 1$ MHz for all the differential spectra. Fig. 2*c* shows the resulting response curve of the sensor measured in this frequency region, which also presents the minimum phase for ΔY. A value of $\Delta G = 8$ nS at $P = 0$ dBm was measured. In analogy with the previous results with silicon [10], the overall response was fitted by a power law $\Delta G = \alpha P^n$ with an exponent $n = 0.85$ (dashed line). A sub-linear relationship of the photoconductivity with optical power has been found both for silicon [13] and III/V semiconductors [14]. This relation can be explained since by increasing light intensity the recombination probability increases, the electron lifetime decreases and the conductivity change induced by the optical absorption becomes less effective [15].

We exploited the characterisation of the sensor response reported above to test the potentiality of the realised CLIPP as in-line power monitor. For this purpose, we progressively changed the optical power P from 0 to −15 dBm (estimated in the ring cavity) and vice versa with discrete steps of 1 dB. Figs. 3*a* and *b* report the corresponding signals simultaneously detected at the output photodiode and from the CLIPP. The measurement was performed with $V_E = 1$ V, $f_E = 100$ kHz and averaging time 1 s. As can be clearly seen, the CLIPP correctly measures all the variations applied at the input power, producing a signal consistent with the photodiode reference curve. In these conditions (1 s averaging time and $V_E = 1$ V), the noise floor of the detection system results to be ∼120 pS rms. The minimum detectable power is approximately −20 dBm, consistent with the characterisation reported in Fig. 2*c*.

The minimum detectable signal depends on the signal/noise ratio (SNR), the signal being determined by L and V_E and the noise depending on the measurement time. Conversely, given a desired level of optical power to be sensed, the size of the CLIPP (i.e. L) can be reduced according to the minimum SNR required for the detection. For instance for $P = 0$ dBm and considering a minimum SNR = 3 (with the same V_E and response time ∼1 s), L can be reduced by 20 times, that is down to 100 μm which represents an acceptable size, compatible with the majority of optical devices to be monitored along the circuit. Smaller CLIPP footprints can be achieved either increasing P or V_E, or increasing the measurement time.

To verify that the CLIPP is mainly sensitive to the light confined within the waveguide, we measured the conductance variation ΔG while moving the input tapered fibre (waist of 1.7 μm) out of the perfect alignment with waveguide core. We shifted the input fibre across about 6 μm in both horizontal and vertical directions, as represented by the dashed lines in the sketch of Fig. 4. The crossing point represents the optimal position to minimise the insertion loss between the fibre and the bus waveguide. For both horizontal and vertical directions, a misalignment of the fibre from the optimum causes a reduction of the fibre–waveguide coupling efficiency and hence reduces the amount of guided power. Consistently, the signal of the CLIPP steeply drops to a nearly

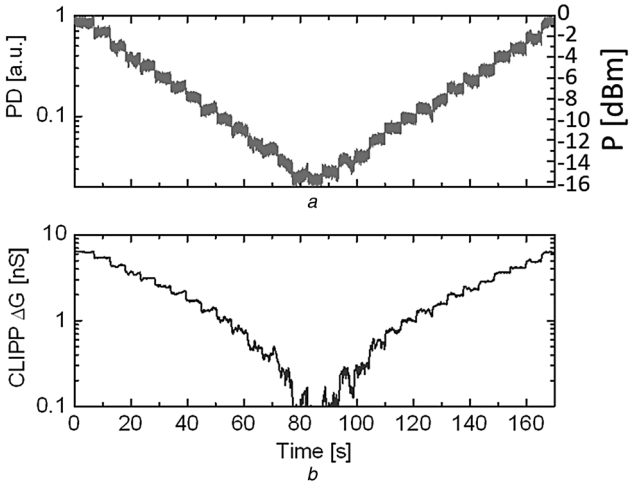

Fig. 3 *Validation of the CLIPP functionality as in-line power monitor*

a Reference photodiode signal detected at the chip output when input power is decreased with steps of 1 dB

b Corresponding ΔG measured with the CLIPP

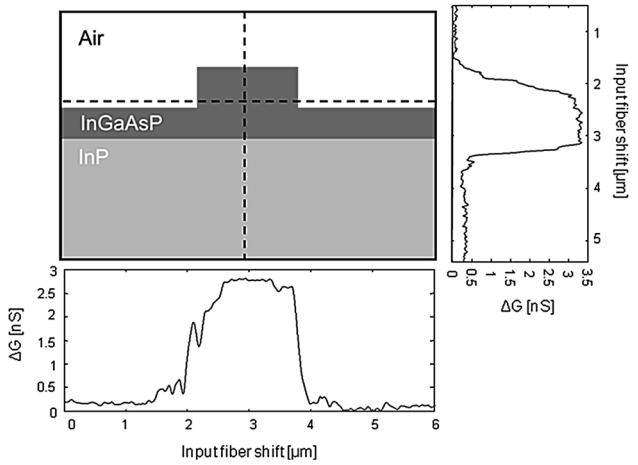

Fig. 4 *CLIPP signal against input fibre shift in the vertical and horizontal directions*

When the tapered fibre (1.7 µm waist) is not perfectly aligned with the waveguide core, the measured ΔG steeply drops

zero value. It is interesting to note that in the vertical direction the alignment of the fibre in the substrate generates a ΔG slightly higher with respect to an alignment in the air on the top of the waveguide, indicating the presence of small residual sensitivity of the CLIPP to weak stray light.

4 Identification of shallow resonances

The realised device provides a useful test bench to demonstrate the potentiality of on-chip non-invasive monitoring of light in the analysis and control of photonic integrated circuits. Thanks to its non-invasive nature, the CLIPP can be integrated inside generic devices, such as ring resonators, enabling to access more accurate information of the device working point compared with conventional external or integrated photodetectors.

As shown in Section 2, the device can be described in terms of two coupled cavities. The first one is represented by the all-pass ring resonator (black ring in Fig. 5*a*). The physical length of the ring (3.736 mm) results in a free spectral range (FSR) of about 184 pm (23 GHz). The simulation of the ring transfer function performed with the commercial circuit simulator Aspic™ [16] showed an operational regime far from the critical coupling condition, with a finesse of the resonant cavity of 3.6 and an extinction ratio of 3 dB. The second resonant cavity of the device is the Fabry–Pérot resonator induced by the chip facets (grey waveguide in Fig. 5*a*), with a FSR of 97 pm (12 GHz). A reflectivity of 28% was simulated for the InP waveguide termination against air since no anti-reflective coating nor angled facets were used. The phase lengths of the two cavities were aligned in the simulation to match the measured data, while the other parameters were directly derived from the standard process design kit of the foundry [17].

Owing to the very low finesse of the ring resonator, the signal of a photodiode placed on the bus waveguide or at the output of the chip cannot be easily used to measure and possibly actively monitor the resonance frequencies of the ring (e.g. to provide a feedback to a thermal actuator). This can be clearly seen in Fig. 5*b*. The black solid line shows the transfer function measured at the chip output with a photodiode while the grey dashed line represents the corresponding simulation, in very good agreement with the measurement. Since the FSR of the ring almost doubles that of the Fabry–Pérot, their mutual interaction causes a periodic disappearing of one of the Fabry–Pérot peaks at the locations of ring notches. The expected positions λ_{FP} for the resonance peaks of the Fabry–Pérot cavity (obtained from simulations) are marked with grey vertical dotted lines. Black dashed lines represent the (simulated) positions λ_R of the resonant notches of the ring resonator. While the former are clearly distinguishable, the latter

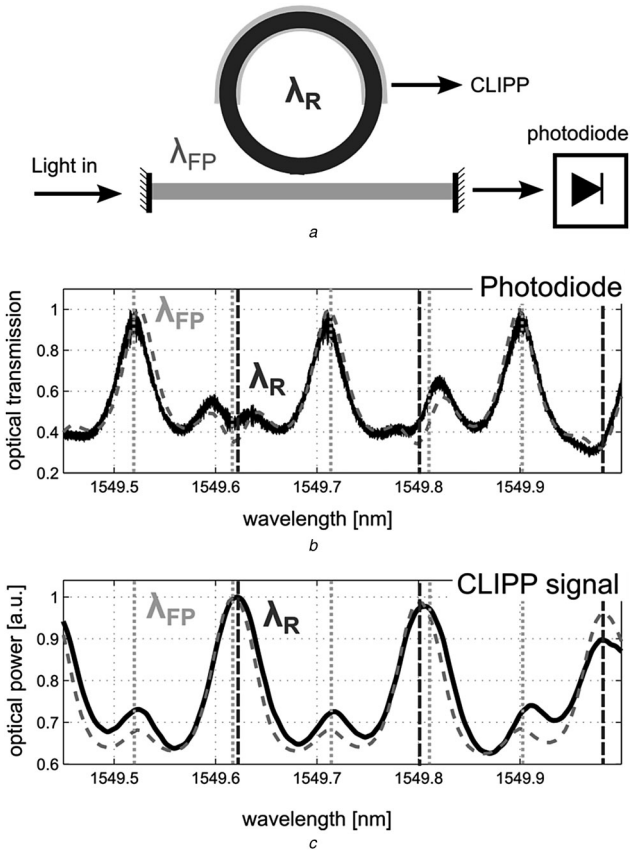

Fig. 5 *Superposition of the resonances of two coupled cavities and power measured at the chip output*

a Superposition of the resonances of two coupled cavities, the Fabry–Pérot (λ_{FP}) induced by the chip facets and the ring resonators (λ_R)
b Power measured at the chip output is shown with black solid line: the fringes of the Fabry–Pérot cavity (green dotted lines) are clearly visible
c CLIPP (black line) is much more sensitive to ring resonances (blue dashed lines)
Simulations (performed with Aspic™ [16]) of the optical power at the chip output and inside the ring (red dashed lines, *b* and *c*, respectively) confirm the experimental results

can be hardly identified and cannot be used to reliably measure the transfer function of the ring.

In this case, it is particularly useful to detect the optical power directly inside the ring cavity, as shown in Fig. 5*c* with grey dashed line. Although at the output port the transfer function of the ring is mostly covered by the effect of the Fabry–Pérot, the simulation of the intra-cavity optical intensity allows to easily identify the ring resonances. The measurement of the power intensity inside the ring was performed by using the CLIPP integrated in the cavity [11] through the curve of Fig. 2*c*. The results (Fig. 5*c*, black solid line) are almost superposed with the simulations. At the ring resonant wavelength λ_R the effect of cavity intensity enhancement is clearly visible and allows to easily detect the transfer function of the ring resonator, unlike the measurement performed through the external photodiode.

5 Conclusions

We have demonstrated that the CLIPP, originally developed on silicon waveguides and devices, can be successfully integrated also on InP-based technologies. This integration did not require any variation to the existing production process and is hence suited for the introduction in a generic platform approach.

Furthermore, the finite conductivity of the InP layer stack allowed to introduce an innovative vertical scheme for the CLIPP. This configuration requires a single sensing metal contact on top of the waveguide and exploits as a large common electrode the back side of the chip. This electrode allows all the CLIPPs to share the

common excitation signal, thus reducing the area of the sensor and the space required by metal pads and electrical connections.

We reported the functionality of the CLIPP as a power monitor able to detect light intensity within the waveguide. We demonstrated that the integration of the CLIPP inside a ring resonator allows to monitor the spectral response of the ring even if highly distorted by an external Fabry–Pérot cavity.

6 Acknowledgments

The authors gratefully acknowledge Franscisco M. Soares, Moritz Baier and Norbert Grote of the Fraunhofer Heinrich Hertz Institut (Berlin) for the fabrication of the devices. This work was partially supported by the European Community's Seventh Framework Programme FP7/2007–2013 under Grant ICT 257210 (PARADIGM) and by the European project BBOI.

7 References

1 Smit, M., Leijtens, X., Ambrosius, H., *et al.*: 'An introduction to InP-based generic integration technology', *Semicond. Sci. Technol.*, 2014, **29**, (8), pp. 083001–083042
2 Baehr-Jones, T., Pinguet, T., Guo-Quiang, P.L., Danziger, S., Prather, D., Hochberg, M.: 'Myths and rumours of silicon photonics', *Nat. Photonics*, 2012, **6**, (4), pp. 206–208
3 Summers, J., Vallaitis, T., Evans, P., *et al.*: 'Monolithic inp-based coherent transmitter photonic integrated circuit with 2.25 Tbit/s capacity', *Electron. Lett.*, 2014, **50**, (16), pp. 1150–1152
4 Norberg, E., Guzzon, R., Nicholes, S., Parker, J., Coldren, L.: 'Programmable photonic lattice filters in InGaAsP–InP', *, IEEE Photonics Technol. Lett.*, 2010, **22**, (2), pp. 109–111
5 Padmaraju, K., Bergman, K.: 'Resolving the thermal challenges for silicon microring resonator devices', *Nanophotonics*, 2013, **2**, pp. 1–14
6 Morichetti, F., Grillanda, S., Melloni, A.: 'Breakthroughs in photonics 2013: toward feedback-controlled integrated photonics', *IEEE Photonics J*, 2014, **6**, (2), pp. 1–6
7 Cho, P.S., Nazarathy, M.: 'Bias control for optical OFDM transmitters', *IEEE Photonics Technol. Lett.*, 2010, **22**, (14), pp. 1030–1032
8 Agarwal, A., Toliver, P., Menendez, R., *et al.*: 'Fully programmable ring-resonator-based integrated photonic circuit for phase coherent applications', *J. Lightwave Technol.*, 2006, **24**, (1), pp. 77–87
9 Miller, D.A.B.: 'Self-configuring universal linear optical component', *Photonics Res.*, 2013, **1**, pp. 1–15
10 Morichetti, F., Grillanda, S., Carminati, M., *et al.*: 'Non-invasive on-chip light observation by contactless waveguide conductivity monitoring', *IEEE J. Sel. Top. Quantum Electron.*, 2014, **20**, pp. 1–10
11 Grillanda, S., Carminati, M., Morichetti, F., *et al.*: 'Non-invasive monitoring and control in silicon photonics using CMOS integrated electronics', *Optica*, 2014, **1**, pp. 129–136
12 Melati, D.: 'A design kit perspective on InP-based photonic integrated circuits'. PhD thesis, Italy, 2014
13 Baehr-Jones, T., Hochberg, M., Scherer, A.: 'Photodetection in silicon beyond the band edge with surface states', *Opt. Exp.*, 2008, **16**, pp. 1659–1668
14 Moustakas, T.D., Misra, M.: 'Origin of the high photoconductive gain in AlGaN films', *Proc. SPIE*, 2007, **6766**, pp. 67660C–67660C-10
15 Rose, A.: 'Concepts in photoconductivity and allied problems' (Interscience Publishers, 1963)
16 Aspic software by Filarete s.r.l, Italy (www.aspicdesign.com)
17 Melati, D., Morichetti, F., Canciamilla, A., *et al.*: 'Validation of the building-block-based approach for the design of photonic integrated circuits', *J. Lightwave Technol.*, 2012, **30**, (23), pp. 3610–3616